Fractional Quantum Hall Phases of Bosons with Tunable Interactions: From the Laughlin Liquid to a Fractional Wigner Crystal

Tobias Graß,[1] Przemyslaw Bienias,[1] Michael J. Gullans,[2] Rex Lundgren,[1] Joseph Maciejko,[3,4,5] and Alexey V. Gorshkov[1,6]

[1]*Joint Quantum Institute, NIST/University of Maryland, College Park, Maryland, 20742, USA*
[2]*Department of Physics, Princeton University, Princeton, New Jersey, 08544, USA*
[3]*Department of Physics, University of Alberta, Edmonton, Alberta T6G 2E1, Canada*
[4]*Theoretical Physics Institute, University of Alberta, Edmonton, Alberta T6G 2E1, Canada*
[5]*Canadian Institute for Advanced Research, Toronto, Ontario M5G 1Z8, Canada*
[6]*Joint Center for Quantum Information and Computer Science, NIST/University of Maryland, College Park, Maryland 20742, USA*

(Received 17 September 2018; published 18 December 2018)

Highly tunable platforms for realizing topological phases of matter are emerging from atomic and photonic systems and offer the prospect of designing interactions between particles. The shape of the potential, besides playing an important role in the competition between different fractional quantum Hall phases, can also trigger the transition to symmetry-broken phases, or even to phases where topological and symmetry-breaking order coexist. Here, we explore the phase diagram of an interacting bosonic model in the lowest Landau level at half filling as two-body interactions are tuned. Apart from the well-known Laughlin liquid, Wigner crystal, stripe, and bubble phases, we also find evidence of a phase that exhibits crystalline order at fractional filling per crystal site. The Laughlin liquid transits into this phase when pairs of bosons strongly repel each other at relative angular momentum $4\hbar$. We show that such interactions can be achieved by dressing ground-state cold atoms with multiple different-parity Rydberg states.

DOI: 10.1103/PhysRevLett.121.253403

Introduction.—In a strong magnetic field, a two-dimensional (2D) electron system can form an incompressible liquid phase exhibiting topological order—that is, order without breaking any symmetry [1]. The Wigner crystal [2,3] competes with this liquid phase and becomes energetically favorable at sufficiently low filling of the lowest ($n = 0$) Landau level (LL) [4,5], or via LL mixing [6]. Other phases with broken symmetry have been predicted for half-filled higher LLs ($n > 1$), using Hartree-Fock calculations [7–9] and exact numerical methods [10,11]. These phases are characterized by stripe or bubble patterns and have been observed in transport experiments [12]. Since the early days of fractional quantum Hall (FQH) physics, there have also been different attempts to describe the FQH effect from a crystal phase ansatz [13,14]. Both fractionally quantized and anisotropic transport has been seen experimentally [15,16], and different field-theoretic approaches describe this incompressible nematic phase in terms of an effective gauge theory [17,18] or assuming the softening of the magnetoroton mode [19,20]. Finally, recent numerical work [21] claims evidence of a FQH phase with nematic order in a microscopic model where the third and the fifth pseudopotentials are comparable to the first one.

While electronic materials offer some knobs to control interactions, e.g., via different substrates or patterned metallic gates, their tunability is rather restricted. Thus, it is tempting to study FQH physics, and the interplay of topological order and symmetry breaking, in alternative systems with tunable interactions. Atomic gases are promising platforms, with the possibility of generating synthetic gauge fields by rotating the system [22] or by optical dressing [23]. More recently, different strategies have also allowed for generating an artificial magnetic field for photons [24]. These systems are often bosonic, but they exhibit similar phases to the electronic systems, including bosonic Laughlin phases and symmetry-broken stripe and bubble phases [25–27]. Strikingly, in such controllable systems, topological transitions between these phases can be induced, e.g., by tuning the scattering length via a Feshbach resonance [25,28], by exploiting confinement-induced resonances [29], or by modifying the pseudopotentials via non-Abelian fields [30,31].

Yet a richer phase diagram is expected in the presence of more than one tuning knob. In this Letter, we study a model with tunable pseudopotentials [21] and consider the bosonic case which is more relevant to atomic, molecular, and optical designer quantum Hall systems. We focus on a system at filling fraction $\nu = 1/2$, restricted to the lowest LL, with fixed contact interaction U_0, and tunable pseudopotentials U_2 and U_4 characterizing the scattering strength between bosons with relative angular momenta $2\hbar$ and $4\hbar$. Using exact diagonalization, we identify

different symmetry-broken phases surrounding the Laughlin liquid. When $U_4 > 0$ becomes sufficiently large, a new phase with striking features is found: The N bosons form a lattice consisting of $2N$ sites, exhibiting a symmetry-protected twofold degeneracy of the ground state at zero momentum. In contrast to the other symmetry-broken phases, the overlap of the ground state with the Laughlin wave function does not drop sharply as the system is tuned from the Laughlin liquid into this new phase. The transition is characterized by a softening of the magnetoroton mode. Finally, we demonstrate an experimental proposal based on ground-state atoms dressed with *multiple* Rydberg states, which enable us to explore a wide range of values of pseudopotentials, including the most interesting one with $U_4 \sim U_0$.

System.—We consider a 2D system of N bosons of mass M subjected to a perpendicular gauge field, whose strength is characterized by the cyclotron frequency ω_c, or equivalently, by the "magnetic" length $l_B \equiv \sqrt{\hbar/M\omega_c}$. The gauge field quenches all bosons into the lowest LL, and interaction between two bosons with relative momentum $\mathbf{q}$ (in units l_B^{-1}) is described by pseudopotentials [32], $U_l = (1/2\pi)^2 \int d\mathbf{q} V_{\mathbf{q}} L_l(|\mathbf{q}|^2) e^{-|\mathbf{q}|^2}$. Here, $V_{\mathbf{q}}$ is the potential, and L_l are Laguerre polynomials. In our model, we fix $U_0 > 0$, and tune U_2 and U_4 from the attractive to the repulsive regime, whereas pseudopotentials with $l > 4$ are neglected. In the numerics, we consider a rectangular system of size $a \times b$ with periodic boundaries (torus). The number of quantized fluxes N_ϕ equals $2N$—that is, $\nu \equiv N/N_\phi = 1/2$. We choose the gauge potential $\mathbf{A}$ in the Landau gauge, $\mathbf{A} \propto (0, x)$, and obtain a single-particle basis of the lowest LL wave functions $\varphi_j(x, y)$ [33]. The quantum number j represents momentum along the y direction.

Evaluating the interaction matrix elements in this basis, we write the Hamiltonian in terms of annihilation or creation operators, $H = \sum_{ijkl} V_{ijkl} a_i^\dagger a_j^\dagger a_k a_l$. The many-body Hilbert space divides into different symmetry sectors: Invariance under magnetic translations leads to conserved (pseudo)momenta K_x [34] and $K_y = \mathrm{mod}\,(\sum_{i=1}^N j_i, N_\phi)$. A sector K_y is connected to $K_y + N_\phi/2$ via a center-of-mass (c.m.) translation, such that the magnetic Brillouin zone (BZ) can be folded onto an $M \times M$ reciprocal lattice's points, with M being the greatest common divisor of N and N_ϕ. Further reduction to the irreducible BZ is possible due to reflection symmetry, leading to an equivalence between $K_{x,y}$ and $-K_{x,y}$ [35].

Numerical results.—Via Lanczos diagonalization, we obtained the low-energy eigenstates of H for up to $N = 10$, varying the parameters $u_2 \equiv U_2/U_0$ and $u_4 \equiv U_4/U_0$. For $u_2 = u_4 = 0$, the Laughlin state is the unique zero-energy ground state at $\mathbf{K} = 0$, and, related by c.m. translation, at $\mathbf{K} = (0, N_\phi/2)$, where units of $(2\pi/a, 2\pi/b)$ are neglected for notational brevity. By evaluating the energy gaps ΔE (both the direct gap at $\mathbf{K} = 0$ and the absolute gap) and the overlap with the Laughlin wave function, we obtain a putative phase diagram in the $u_2 - u_4$ space; see Fig. 1. The Laughlin phase is surrounded by phases of broken symmetry with (quasi)degenerate ground states in different symmetry sectors. A pronounced finite-size gap occurs when $|u_4|$ is large and attractive; see Fig. 1(b).

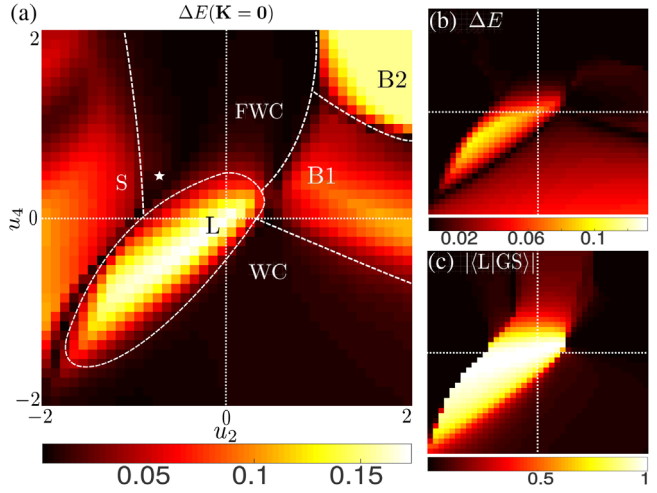

FIG. 1. (a) Energy gap ΔE at $\mathbf{K} = 0$ as a function of the pseudopotentials. The inferred phase diagram is indicated by white dashed lines. The Laughlin phase (L) is surrounded by a stripe phase (S), bubble phases ($B1$ and $B2$), an integer Wigner crystal (WC) phase, and a fractional Wigner crystal (FWC) phase. The star indicates the point for which the experimental realization is discussed in detail. (b) The absolute energy gap versus u_2 and u_4: Small gaps indicate a symmetry-broken phase, in contrast to the larger gaps seen in the Laughlin liquid phase. (c) The overlap with the Laughlin wave function versus u_2 and u_4: Nonzero overlap persists in the FWC phase. All data were obtained for eight bosons on a torus with ratio $a/b = 0.9$.

To identify the order of each phase, we analyze the ground-state pair-correlation function $g_2(z) \propto \langle \sum_{i \neq j} \delta(z - z_i + z_j) \rangle$, where $z \equiv x + iy$; see Fig. 2. The Laughlin liquid stands out through perfect anticorrelations, $g_2(0) = 0$, and a homogeneous particle distribution [Fig. 2(f)]. When u_2 is repulsive and sufficiently strong, clustered lattice configurations become favorable [Figs. 2(c) and 2(d)]. Such "bubble" phases are also expected for electronic systems in higher LLs [7–11], dipolar gases [25], and Rydberg systems [27]. A configuration consisting of a single cluster along one direction appears when u_2 is attractive [Fig. 2(e)]. In the case of an attractive u_4 potential, we find a square crystal arrangement with one boson per site [Fig. 2(b)]. Of course, compressible phases depend also on the system geometry, chosen as $a/b = 0.9$ and $N = 8$. Similar results obtained for other system sizes are presented in the Supplemental Material [36].

We now turn our attention to the interesting behavior found when u_4 is strong and repulsive [Fig. 2(a)]: The

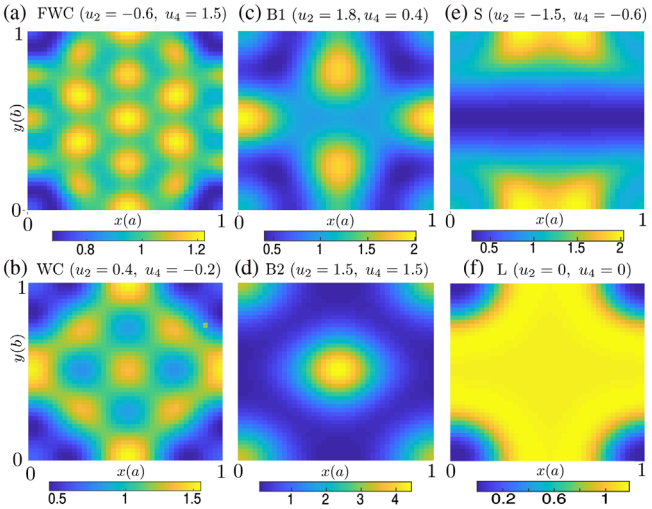

FIG. 2. The ground-state pair-correlation function $g_2(x, y)$ for $N = 8$ and $a/b = 0.9$ for different u_2 and u_4 corresponding to the different phases: (a) triangular lattice with $1/2$ boson per lattice site (fractional Wigner crystal), (b) square lattice with 1 boson per site (Wigner crystal), (c) triangular arrangement of "bubbles" (2 bosons per bubble), (d) square arrangement of "bubbles" (4 bosons per bubble), (e) clustering along the x axis (stripe), and (f) homogeneous Laughlin liquid.

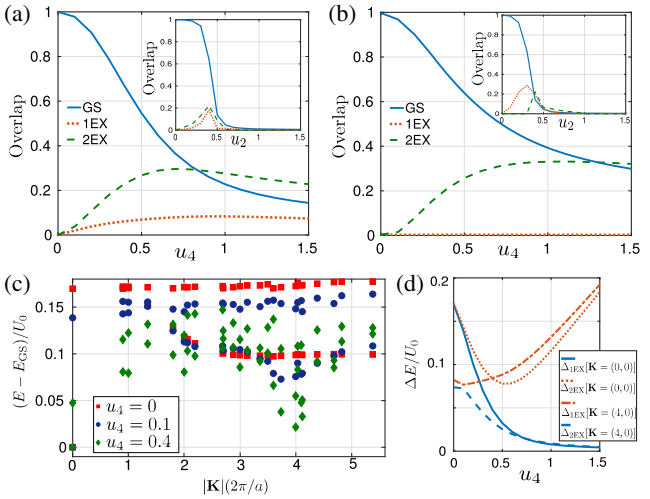

FIG. 3. (a) Energy of the lowest two eigenstates at each $\mathbf{K}$, for different u_4 (with $u_2 = 0$). Increasing u_4 softens the magnetoroton branch around $\mathbf{K} = (4, 0)$ and $\mathbf{K} = (2, 4)$. (b) Direct energy gaps Δ_{1EX} and Δ_{2EX} of the first and second excited states at $\mathbf{K} = 0$ and $\mathbf{K} = (4, 0)$, as a function of u_4 (with $u_2 = 0$). (c) Overlap between the Laughlin state and the three lowest eigenstates ($\mathbf{K} = 0$) of H as a function of u_4, with $u_2 = 0$. The transition into the FWC phase ($u_4 \approx 0.5$) occurs without a sudden drop of the overlap, in contrast to the transition into a bubble phase shown in the inset (overlap vs u_2, with $u_4 = 0$). (b) Overlap between the Laughlin magnetoroton state at $\mathbf{K} = (4, 0)$ and the three lowest eigenstates. All data in (a–d) was obtained for $N = 8$ and $a/b = 0.9$.

pair-correlation function shows a triangular lattice structure with $2N - 1$ peaks (plus a deep valley at $z = 0$), so we call it a "fractional Wigner crystal" (FWC). A half-filled crystal exhibits quantum fluctuations and frustration, and one might speculate that the bosons have fractionalized into semions forming a lattice at filling 1. The transition from the Laughlin liquid into the FWC phase suggests a close relation between the FQH and the FWC phases: As shown in Fig. 3(a), the FWC phase arises through a softening of the magnetoroton mode, a collective excitation branch obtained by a long-wavelength density modulation of the Laughlin state [37]. Finite values of u_4 soften this branch near $|\mathbf{K}|a/(2\pi) \approx 4$, and degeneracy with the $\mathbf{K} = 0$ ground state occurs at $u_4 \approx 0.5$, giving rise to a symmetry-broken phase. In the same regime, the first excited state at $\mathbf{K} = 0$ becomes quasidegenerate, too, and for $u_4 \approx 0.5$ the direct gap to the second excited state is minimal; see Fig. 3(b). The overlaps of the FWC ground states with the Laughlin wave function at $\mathbf{K} = 0$ [see Fig. 3(c)] and with the Laughlin magnetoroton state at $\mathbf{K} = (4, 0)$ [see Fig. 3(d)] decay smoothly as u_4 is increased, but they remain finite even deep in the FWC phase. This behavior is in sharp contrast to the behavior at the boundary between the Laughlin and bubble phases, shown in the insets of Figs. 3(c) and 3(d): Upon increasing u_2 at $u_4 = 0$, a sudden drop of the overlap to values near zero occurs at the phase boundary. These observations suggest that Laughlin-like behavior remains present in the ground and excited states of the FWC phase.

A characteristic feature of each symmetry-broken phase is its tower of states [38,39]—that is, the structure of the quantum numbers of the degenerate ground states. This structure reflects the order seen in the pair-correlation function: The triangular bubble phase ($B1$) [Fig. 2(c)] has degenerate ground states (for $N = 8$) at reciprocal lattice vectors $\mathbf{K}_{mn} = m(2, 1) + n(2, -1)$, the square bubble phase ($B2$) [Fig. 2(d)] at $\mathbf{K}_{mn} = m(1, 1) + n(1, -1)$, and the stripe phase ($S$) [Fig. 2(e)] at $\mathbf{K}_m = m(0, 1)$. In the FWC phase, the ground states form a pair of stripes winding twice around the folded magnetic Brillouin zone; see Fig. 4. In contrast to conventional stripe phases,

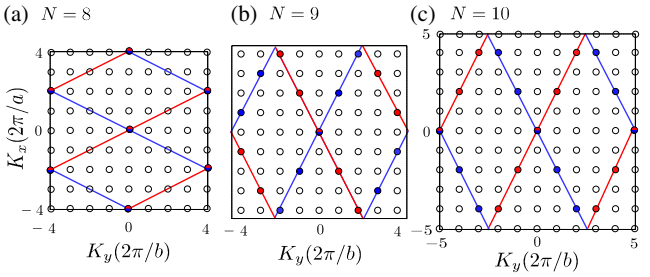

FIG. 4. We plot the folded magnetic Brillouin zone for different N and mark with filled circles the symmetry sectors belonging to the ground-state manifold in the FWC phase. Doubly degenerate sectors are filled with two colors. The ground states form two stripes (red and blue solid lines), related to each other via reflection, winding twice around the zone.

the stripes are not parallel to a symmetry axis of the torus, but they are parametrized as $\mathbf{K}_m^{i\pm} = m(k_x^i, \pm k_y^i)$, with $k_x^i \neq 0 \neq k_y^i$. The pairwise occurrence of these stripes is demanded by reflection symmetry and leads to characteristic double degeneracies at reciprocal lattice points where the stripes cross. For $N = 8$, the two stripes describe exactly the same set of points, and the ground-state pattern in reciprocal space matches with a triangular structure, also seen in the correlation function for $N = 8$ [Fig. 2(a)]. In contrast, for $N = 9$ and 10, stripe crossings coincide with reciprocal lattice points only at $\mathbf{K} = (0, 0)$. Accordingly, also the correlation function deviates from the regular lattice structure (see the Supplemental Material [36]), but it still exhibits $2N - 1$ peaks.

Experimental realization.—The phases discussed above can be realized using cold ground-state alkaline atoms dressed with Rydberg states [40,41] in a synthetic magnetic field generated by rotating the system [22]. Typical interactions between s-state Rydberg-dressed atoms [dashed green curve in Fig. 5(a)] saturate for distances smaller than the so-called Rydberg blockade radius, a phenomenon studied in the context of FQH states in Ref. [27]. For dressing with Rydberg p states, the interaction can be nonmonotonic [solid orange curve in Fig. 5(a)] as a function of distance [42,43]. Each of these two cases enables us to explore part of the phase diagram; however, in order to access the FWC regime we need even more flexibility in the shape of interactions. We propose to combine the s- and p-state dressings to achieve a hump-dip-hump potential [dot-dashed curve in Fig. 5(a)].

As an example [see Fig. 5(b)], we consider ground-state $|g\rangle = |F = 2, m_F = 2\rangle$ atoms of ^{87}Rb weakly dressed with two Rydberg states: (i) an $n_pP_{1/2}$ state $|+\rangle = |n_p, m_J = 1/2\rangle$ using a laser field with Rabi frequency $2\Omega_p$ and detuning δ_+,

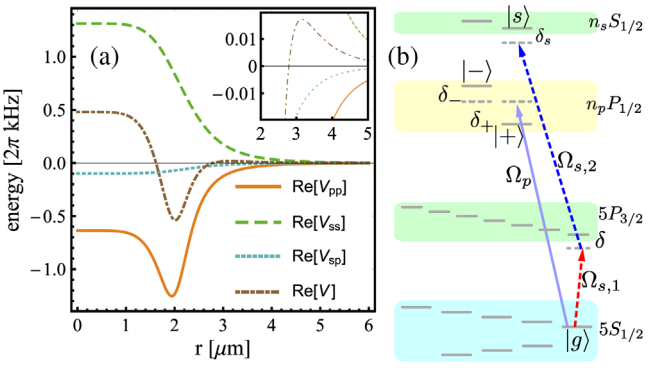

FIG. 5. Experimental realization. (a) The s and sp dressing lead to a standard soft-core potential (green and blue dashed lines, respectively), whereas p dressing leads to the potential with a sharp dip (orange solid line). Together they lead to a hump-dip-hump potential (brown dot-dashed line). The outer hump, relevant for ensuring that $U_4 > 0$, is shown in the inset. (b) Level scheme for the dressing of the ground state $|g\rangle$ with Rydberg states $|s\rangle$ and $|+\rangle$.

and (ii) an $n_sS_{1/2}$ state $|s\rangle = |n_s, m_S = 1/2\rangle$ using an effective Rabi frequency $2\Omega_s$ and detuning δ_s. The coupling to $|s\rangle$ is achieved using a two-photon transition with single-photon detuning δ and two Rabi frequencies $2\Omega_{s,1}$, $2\Omega_{s,2} \ll |\delta|$, leading to $\Omega_s = -\Omega_{s,1}\Omega_{s,2}/\delta$. Without interactions and for $|(\Omega_{s/p}/\delta_{s/p})| \ll 1$, the dressed state takes the form $|d\rangle = |g\rangle - (\Omega_s/\delta_s)|s\rangle - (\Omega_p/\delta_p)|+\rangle$. For weak dressing, the total two-body interaction $V(r)$ between two $|d\rangle$ states is a sum over separately calculated potentials, $V = V_{pp} + V_{ss} + 2V_{sp}$, where $V_{aa'}$ arises due to the interaction of Rydberg states a and a'.

By choosing $|n_p - n_s| \gg 1$, we can neglect direct dipolar coupling between two-atom states $|s\pm\rangle$ and $|\pm s\rangle$ (where $|-\rangle = |n_p, m_J = -1/2\rangle$) and describe the interactions using only diagonal van der Waals (vdW) potentials. The vdW interaction between $|\pm\rangle$, assuming a magnetic field perpendicular to the 2D plane, is

$$\frac{1}{r^6}\begin{pmatrix} \alpha-\beta & 0 & 0 & \beta \\ 0 & \alpha+\frac{\beta}{3} & -\frac{\beta}{3} & 0 \\ 0 & -\frac{\beta}{3} & \alpha+\frac{\beta}{3} & 0 \\ \beta & 0 & 0 & \alpha-\beta \end{pmatrix} \tag{1}$$

in the $\{++, +-, -+, --\}$ basis, with $\alpha/2\pi = 690.2\ \mathrm{MHz}\,\mu\mathrm{m}^6$ and $\beta/2\pi = 6204.3\ \mathrm{MHz}\,\mu\mathrm{m}^6$ for $n_p = 62$. This leads to the effective interaction V_{pp} between the p components of the dressed state, which, within a fourth-order perturbation calculation, equals ($\hbar = 1$)

$$\frac{2\Omega_p^4[\alpha(\alpha-2\beta) + 2\delta_- r^6(\alpha-\beta)]}{\delta_+^3\{\alpha(\alpha-2\beta) + 2r^6[\delta_+(\alpha-\beta) + \delta_-(\alpha-\beta+2\delta_+ r^6)]\}}.$$

The interactions V_{ss} and V_{sp} arise from the standard dressing of each ground-state atom with a single Rydberg level interacting via a vdW C_6/r^6 potential. In this case, the interaction takes the form

$$\frac{C_6(\delta_1+\delta_2)\Omega_1^2\Omega_2^2}{\delta_1^2\delta_2^2[C_6 + (\delta_1+\delta_2)r^6]}, \tag{2}$$

where, for V_{ss}, we set $\delta_1 = \delta_2 = \delta_s$, $\Omega_1 = \Omega_2 = \Omega_s$, and $C_6 = C_{ss}$, while, for V_{sp}, we set $\delta_1 = \delta_s$, $\delta_2 = \delta_+$, $\Omega_1 = \Omega_s$, $\Omega_2 = \Omega_p$, and $C_6 = C_{sp}$.

The strength of V_{ss} and V_{sp} relative to V_{pp} can be tuned via Rabi frequencies, detunings, and principal quantum number n_s. By setting $\delta_+/2\pi = -21.41$ MHz, $\delta_-/2\pi = 16.15$ MHz, we achieve a resonance-free hump-dip V_{pp} potential [43], and by choosing $\delta_s/2\pi = 17.28$ MHz and $n_s = 52$, such that $C_{sp}/(2\pi\ \mathrm{MHz}\,\mu\mathrm{m}^6) = -682.08 < 0$ and $C_{ss}/(2\pi\ \mathrm{MHz}\,\mu\mathrm{m}^6) = 3918.89 > 0$, the other two potentials are also resonance-free, and V_{sp} is

much weaker than V_{ss}, with Rydberg blockade radius between s states $r_{ss} = 2.2\ \mu$m [44]. We choose $l_B = 2\ \mu\text{m} \sim r_{ss}$, so that we can neglect U_j for $j > 4$. By choosing optimal Rabi frequencies, we can still operate in a weakly dressed regime and simultaneously access the hardest-to-achieve regime of strong U_4, corresponding to the hump-dip-hump potential in Fig. 5(a). Specifically, for $\Omega_p/(2\pi) = 1.32933$ MHz and $\Omega_s/(2\pi) = 1.35679$ MHz, we get $\{u_2, u_4, u_6\} = \{-0.72, 0.45, 0.11\}$ with $U_0/2\pi = 0.00061$ kHz and $\text{Im}[U_l]/\text{Re}[U_l] < 0.01$. Finally, if the LL gap ω_c is larger than the intra-LL pseudopotentials and the relevant inter-LL interactions (both are $\sim U_0$), we can neglect higher LLs. For $l_B = 2\ \mu$m, this is indeed the case, $U_0 \ll \omega_c = 2\pi \times 0.029$ kHz. By changing the detunings and Rabi frequencies and possibly varying them in time, one can investigate other phases of the phase diagram in Fig. 1 and study transitions between them.

Summary.—We studied a FQH system that exhibits a density modulation when higher pseudopotentials (in particular U_4) are on the order of U_0 and proposed realizing such exotic interactions with Rydberg-dressed atoms. Our scheme allows us to explore FQH scenarios beyond those found in electronic systems with Coulomb interactions. Our findings point towards an interplay of two fundamental concepts, topological order and symmetry breaking, which both appear to be present in our system. Whether and how the concepts to classify topological quantum liquids can be applied to the crystal phase is an interesting subject for future studies. Some numerical results for the entanglement entropy [45–47] are provided in the Supplemental Material [36].

We acknowledge discussions with R. Belyansky, A. Gromov, and S. Sondhi. T. G. acknowledges funding by the NSF through the Physics Frontiers Center at the Joint Quantum Institute. R. L. is supported by a NIST NRC Research Postdoctoral Associateship Award. P. B., R. L., and A. V. G. acknowledge funding by AFOSR, NSF Physics Frontiers Center at the Joint Quantum Institute, ARO, ARO MURI, ARL CDQI, NSF Ideas Lab, Department of Energy ASCR Quantum Testbed Pathfinder program, and Department of Energy BES Materials and Chemical Sciences Research for Quantum Information Science program. J. M. was supported by NSERC Grant No. RGPIN-2014-4608, the CRC Program, CIFAR, and the University of Alberta. The authors acknowledge the University of Maryland supercomputing resources made available for conducting the research reported in this Letter.

[1] R. B. Laughlin, Phys. Rev. Lett. **50**, 1395 (1983).
[2] E. Wigner, Phys. Rev. **46**, 1002 (1934).
[3] H. Deng, Y. Liu, I. Jo, L. N. Pfeiffer, K. W. West, K. W. Baldwin, and M. Shayegan, Phys. Rev. Lett. **117**, 096601 (2016).
[4] D. Yoshioka and H. Fukuyama, J. Phys. Soc. Jpn. **47**, 394 (1979).
[5] P. K. Lam and S. M. Girvin, Phys. Rev. B **30**, 473 (1984).
[6] J. Zhao, Y. Zhang, and J. K. Jain, Phys. Rev. Lett. **121**, 116802 (2018).
[7] A. A. Koulakov, M. M. Fogler, and B. I. Shklovskii, Phys. Rev. Lett. **76**, 499 (1996).
[8] M. M. Fogler and A. A. Koulakov, Phys. Rev. B **55**, 9326 (1997).
[9] E. Fradkin and S. A. Kivelson, Phys. Rev. B **59**, 8065 (1999).
[10] E. H. Rezayi, F. D. M. Haldane, and K. Yang, Phys. Rev. Lett. **83**, 1219 (1999).
[11] F. D. M. Haldane, E. H. Rezayi, and K. Yang, Phys. Rev. Lett. **85**, 5396 (2000).
[12] M. P. Lilly, K. B. Cooper, J. P. Eisenstein, L. N. Pfeiffer, and K. W. West, Phys. Rev. Lett. **82**, 394 (1999).
[13] S. Kivelson, C. Kallin, D. P. Arovas, and J. R. Schrieffer, Phys. Rev. Lett. **56**, 873 (1986).
[14] Z. Tešanović, F. Axel, and B. I. Halperin, Phys. Rev. B **39**, 8525 (1989).
[15] J. Xia, J. P. Eisenstein, L. N. Pfeiffer, and K. W. West, Nat. Phys. **7**, 845 (2011).
[16] N. Samkharadze, K. A. Schreiber, G. C. Gardner, M. J. Manfra, E. Fradkin, and G. A. Csáthy, Nat. Phys. **12**, 191 (2016).
[17] M. Mulligan, C. Nayak, and S. Kachru, Phys. Rev. B **82**, 085102 (2010).
[18] M. Mulligan, C. Nayak, and S. Kachru, Phys. Rev. B **84**, 195124 (2011).
[19] J. Maciejko, B. Hsu, S. A. Kivelson, Y. J. Park, and S. L. Sondhi, Phys. Rev. B **88**, 125137 (2013).
[20] Y. You, G. Y. Cho, and E. Fradkin, Phys. Rev. X **4**, 041050 (2014).
[21] N. Regnault, J. Maciejko, S. A. Kivelson, and S. L. Sondhi, Phys. Rev. B **96**, 035150 (2017).
[22] N. Cooper, Adv. Phys. **57**, 539 (2008).
[23] N. Goldman, G. Juzelinas, P. Öhberg, and I. B. Spielman, Rep. Prog. Phys. **77**, 126401 (2014).
[24] T. Ozawa *et al.*, arXiv:1802.04173.
[25] N. R. Cooper, E. H. Rezayi, and S. H. Simon, Phys. Rev. Lett. **95**, 200402 (2005).
[26] H. Seki and K. Ino, Phys. Rev. A **77**, 063602 (2008).
[27] F. Grusdt and M. Fleischhauer, Phys. Rev. A **87**, 043628 (2013).
[28] C. Repellin, T. Yefsah, and A. Sterdyniak, Phys. Rev. B **96**, 161111 (2017).
[29] B. Juliá-Díaz, T. Graß, O. Dutta, D. Chang, and M. Lewenstein, Nat. Commun. **4**, 2046 (2013).
[30] S. Komineas and N. R. Cooper, Phys. Rev. A **85**, 053623 (2012).
[31] M. Burrello, M. Rizzi, M. Roncaglia, and A. Trombettoni, Phys. Rev. B **91**, 115117 (2015).
[32] F. D. M. Haldane, Phys. Rev. Lett. **51**, 605 (1983).
[33] D. Yoshioka, B. I. Halperin, and P. A. Lee, Phys. Rev. Lett. **50**, 1219 (1983).
[34] F. D. M. Haldane, Phys. Rev. Lett. **55**, 2095 (1985).
[35] An additional C_4 symmetry is only present for the special case of a square system, $a/b = 1$.

[36] See Supplemental Material at http://link.aps.org/supplemental/10.1103/PhysRevLett.121.253403 for the dependence of numerical results on system size and geometry.
[37] S. M. Girvin, A. H. MacDonald, and P. M. Platzman, Phys. Rev. B **33**, 2481 (1986).
[38] P. W. Anderson, Phys. Rev. **86**, 694 (1952).
[39] A. M. Laeuchli, M. Schuler, and A. Wietek, Studying continuous symmetry breaking with exact diagonalization, in *Quantum Materials: Experiment and Theory Modeling and Simulation*, edited by E. Pavarini, E. Koch, J. van den Brink, and G. Sawatzky (Forschungszentrum Jülich, Jülich, 2016), Vol. 6.
[40] M. Saffman, T. G. Walker, and K. Mølmer, Rev. Mod. Phys. **82**, 2313 (2010).
[41] R. Löw, H. Weimer, J. Nipper, J. B. Balewski, B. Butscher, H. P. Büchler, and T. Pfau, J. Phys. B **45**, 113001 (2012).
[42] R. M. W. van Bijnen and T. Pohl, Phys. Rev. Lett. **114**, 243002 (2015).
[43] A. W. Glaetzle, M. Dalmonte, R. Nath, C. Gross, I. Bloch, and P. Zoller, Phys. Rev. Lett. **114**, 173002 (2015).
[44] In our case, the hyperfine splitting in the n_pP manifold is $\Delta_{hfs,n_p} \approx 0.4$ GHz, which means that the corrections to the vdW potential can be significant. Nevertheless, we expect that our results should hold qualitatively and, moreover, by working with smaller $\delta_\pm$ and δ_s, we can ensure that the corrections to the vdW potential will be weaker.
[45] A. Kitaev and J. Preskill, Phys. Rev. Lett. **96**, 110404 (2006).
[46] M. Levin and X.-G. Wen, Phys. Rev. Lett. **96**, 110405 (2006).
[47] A. M. Läuchli, E. J. Bergholtz, and M. Haque, New J. Phys. **12**, 075004 (2010).